Progress In Electromagnetics Research B, Vol. 57, 279–298, 2014

Land-Buried Object Detection and Target-Shape Recognition in Lossy and Dispersive Soil

Khalid M. Ibrahim[1, *], Khalid F. A. Hussein[2], and Abd-El-Hadi A. Ammar[3]

Abstract—In this paper, a simulation of ground penetrating radar "GPR" system on lossy and dispersive soil is investigated. The capability of the GPR system to detect buried targets is examined by evaluating and comparing the electromagnetic coupling between the transmitting and receiving antennas in two cases: (i) when the system is placed over an empty ground and (ii) when it is placed over a ground inside which a practical target is buried at a proper depth. Simulation software based on the finite difference time domain "XFDTD" is used for the electromagnetic simulations. The results concerning the coupling between the transmitting and receiving antennas are presented considering various practical parameters such as the operating frequency, the electric properties of the ground soil and the buried target, and the location at which the receiving element is placed. It is shown that the target detectability is strongly dependent on all of the above parameters. Also, the capability of target shape extraction and recognition are demonstrated through polarimetric ground penetrating radar.

1. INTRODUCTION

Realistic modeling of a ground penetrating radar system has to deal with many aspects such as lossy and dispersive media in the ground, target geometry, and natural clutter like roots and rocks. Numerical simulations of GPR systems are particularly important for the development of GPR antennas, detection techniques and detection algorithms. The finite difference time domain (FDTD) method is a powerful computational electromagnetic numerical technique widely used for this type of applications. It has the capability of modeling lossy and dispersive material as well as antennas [1, 2]. The performance of the GPR sensor strongly depends on the dielectric properties of the soil, which in turn are related to specific parameters, such as texture, bulk density, and water content. The accurate knowledge of soil dielectric constant is of primary importance in this kind of radar application and is particularly difficult to achieve in the presence of dispersive media, where the dielectric properties vary with frequency. The electromagnetic wave reflection from dispersive media has been a subject of interest to researchers for many years [3–7].

This paper provides elaborate discussions, based on accurate results, to investigate the capability of the polarimetric GPR sensor described in [8, 9] to detect buried targets in lossy and dispersive soil using a Gaussian pulse excitation applied at the feed point of the sensor transmitting antenna. The increase in the electromagnetic coupling between the transmitting and receiving antennas of the sensor due to the presence of the target is used as a measure of the system capability. Two dispersive soil models are simulated to demonstrate the dispersion effects on the target detection capability.

The present work produces the results of extracting the buried object shape from the co-polarization channels (xx and yy) data collected from the polarimetric GPR system. For the target shape recognition, the extracted shape curve is compared with the reference target shape curve when its centroid coincident with each other, and then a least-squared error method is applied to take the match or mismatch decision

Received 13 November 2013, Accepted 18 December 2013, Scheduled 25 December 2013

* Corresponding author: Khalid Moustafa Ibrahim (khaledmus@gmail.com).

[1] Microwave Engineering Department, Electronics Research Institute, Cairo, Egypt. [2] Microwave Engineering Department, Electronics Research Institute, Cairo, Egypt. [3] Electronics and Electrical Communications Department, Faculty of Engineering, El-AZHAR University, Cairo, Egypt.

with a specific reference target shape. The match or mismatch decision is taken based of the relative error defined as the ratio between the dashed area shown in Fig. 1 and the area enclosed by the boundary of the original target shape curve

$$\hat{e} = \frac{e}{A} \tag{1}$$

where e is the area subtended between the reference and retrieved curves (shown as dashed area in Fig. 1) and A the area of enclosed by the reference curve.

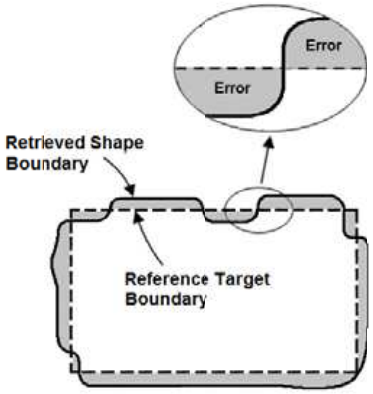

Figure 1. Target shape recognition is achieved by comparing the retrieved shape to the original shape.

The mathematical and numerical algorithms for extracting the buried object shape and recognizing the shape of a reference target with calculating the relative mismatch error are described in details in [8, 9].

2. DISPERSIVE MATERIALS AND THE DISPERSIVE SOIL MODELING

All materials are, to some extent, dispersive. If a field applied to a material undergoes a sufficient rapid change, there is a time lag in the response of the polarization or magnetization of the atoms. It has been found that such materials have complex, frequency dependent constitutive parameters. On the one hand, the lossy material is dispersive since it has a complex, frequency dependent permittivity. On the other hand, the Kronig-Kramers relations imply that if the constitutive parameters of a material are frequency dependent, they must have both real and imaginary parts [10]. Such a material, if isotropic, must be lossy. So dispersive materials are general lossy and must have both dissipative and energy storage characteristics. However, many materials have frequency range called transparency ranges over which the imaginary parts are smaller than the real parts of constitutive parameters. If we restrict our interest to these ranges, we may approximate the material as lossless. Numerous researchers have demonstrated that Lorentz, Debye and Cole-Cole models can be used to accurately predict dispersive properties of many media [11].

The Lorentz material is a good model for many materials encountered in optics and engineering. A compact form for both TE and TM reflection coefficients ware is presented in [12, 13], which provide useful intuition about the response of a Lorentz medium half space. The Debye model is utilized to describe the frequency behavior of the permittivity of many types of materials, especially polar liquids. This model has been extended to include conductivity and several relaxation components, and used to describe the behavior of such diverse materials as biological tissues, building materials, circuit boards and ceramics [11]. Another model commonly used to capture the relaxation-based dispersive properties is the Cole-Cole model that is more general than the Debye model. For many types of materials including biological tissues, the Cole-Cole models provide an excellent fit to experimental data over the entire measurement frequency range. However, to our knowledge, the time-domain reflection coefficient of a Cole-Cole half space for any polarization is not available so far, perhaps due to the computational complexity of embedding a Cole-Cole dispersion model into numerical methods [11].

Although the determination of the dielectric properties of earth materials remains largely experimental, there is always the need of soil modeling. Experimental data indicate that dielectric behavior of wet snow, rocks, soils and even dry sand follows the Debye relaxation [14, 15]. This good fit to the Debye model is explained by the natural occurring of moisture in varying proportions in almost every earth material. The complex relative permittivity $\varepsilon_r(\omega)$ of the first-order Debye dispersion is described by the following equation

$$\varepsilon_r(\omega) = \varepsilon_\infty + \frac{\varepsilon_S - \varepsilon_\infty}{1 + j\omega\tau} + \frac{\sigma_S}{j\omega\varepsilon_0} \tag{2}$$

where, ω is the angular frequency, ε_∞ the relative permittivity at $\omega = \infty$, ε_S the relative permittivity at DC, ε_0 the permittivity of free space, τ the Debye relaxation time, and σ_S the static electric conductivity.

Simulations are done for a realistic soil described as "Puerto Rico clay loams soil, with moisture content 10%", whose dispersive properties have been characterized experimentally in [16]. These soil properties are modeled by the first-order Debye model described in Equation (2). The Puerto Rico clay loams relative permittivity $\varepsilon_r(\omega)$ shown in Fig. 2 was giving by fitting the modeled parameters obtained in Table 1. As shown in this figure, there is a considerable variation in the relative permittivity with the frequency in the frequency band 100 MHz to 3 GHz and very small variation in the frequency band 4 GHz to 10 GHz, so that the dispersion effects does not clear at the high frequencies. Also, the maximum loss occurs at the relaxation frequency, 700 MHz.

A hypothetical dispersive soil type was considered to demonstrate the dispersion effects at high frequencies, and its properties are modeled also by the first-order Debye model described in Equation (2). The soil relative permittivity $\varepsilon_r(\omega)$ shown in Fig. 3 was given by fitting the modeled parameters obtained in Table 2. As shown in this figure, there is a variation in the relative permittivity with the frequency at all frequencies over the frequency band 100 MHz to 10 GHz, so that the dispersion effects are clear at the high frequencies. There is laxation frequency at which the maximum loss occurs is 7.2 GHz.

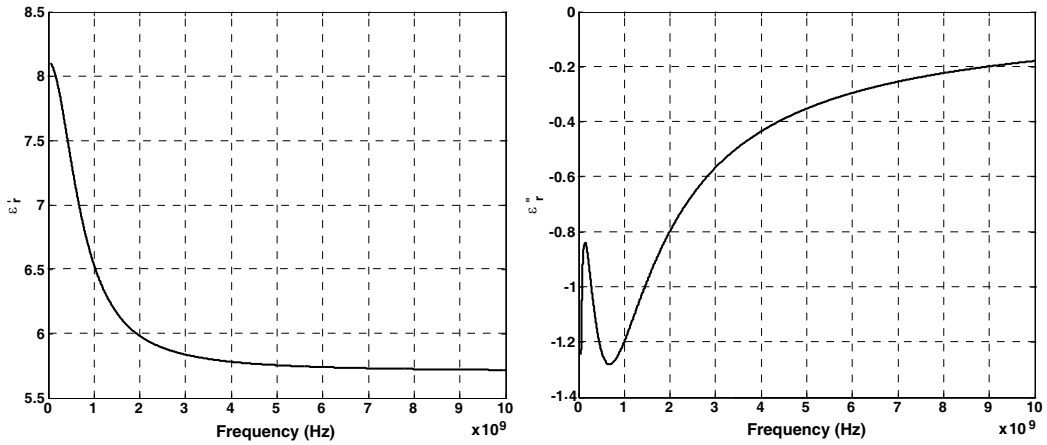

Figure 2. The relative permittivity of the Puerto Rico clay loams with 10% moisture content.

Table 1. Model parameters for Puerto Rico clay loams.

ε_∞	ε_S	τ (ns)	σ_S (mS/m)
5.706	8.1118	0.22	3.022

Table 2. Model parameters for hypothetical dispersive soil.

ε_∞	ε_S	τ (ns)	σ_S (mS/m)
5.706	8.1118	0.022	3.022

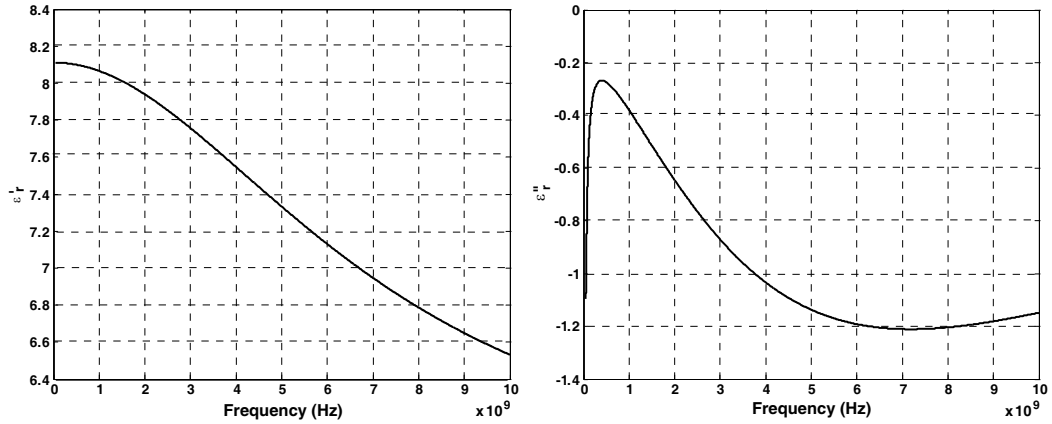

Figure 3. The relative permittivity of the hypothetical dispersive soil.

3. POLARIMETRIC GPR SENSOR CONSTRUCTION AND OPERATION

A polarimetric GPR sensor has been used in GPR system [8, 9], which consists of a clustered two-dimensional planar array of $M \times N$ coplanar crossed-dipole antennas. For example, a cluster composed of 7×7 elements is shown in Fig. 4(a). The element of a cluster is composed of an x-oriented dipole crossed with another y-oriented dipole. All the elements of a cluster act as receiving antennas except for the central one which is housed in a conducting reflector and acts as a transmitter for illuminating the rectangular area just below the corresponding cluster of the antenna array. As shown in Fig. 4(b), the conducting housing over the transmitting crossed-dipole is a partial cover made to prevent direct coupling between the transmitting antenna and all the receiving antennas as well as to prevent the radiation into the upper half space. The construction and dimensions of the transmitting element housed in metallic reflector are shown in Fig. 5. When the sensor is placed over empty ground, the coupling between the transmitting antenna '1' and a receiving antenna '2', $|S_{21}|$, is very small. As the sensor is placed over a soil with an object buried near enough to the ground surface, the inhomogeneity occurring due to the difference between the electromagnetic properties of the soil and that of the buried object leads to scattering a portion of the signal radiated by the transmitting antenna to the receiving antenna and, thereby, increasing the coupling between the transmitting and receiving antennas. Thus, the increase in the electromagnetic coupling can be used to indicate the presence of an inhomogeneity just below the receiving dipole. If enough number of closely spaced receiving elements are regularly

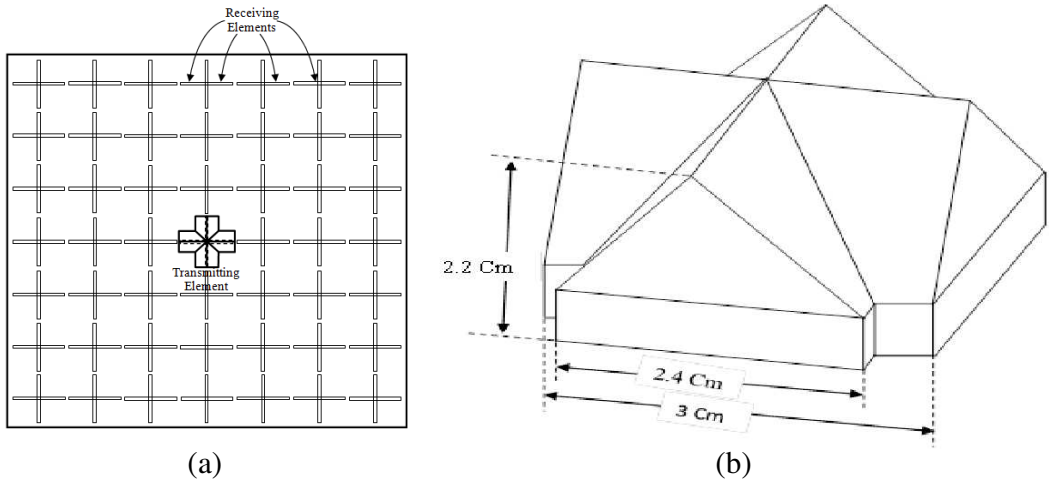

Figure 4. A cluster of GPR antenna system composed of 7×7 antenna elements. (a) GPR antenna system. (b) Conducting reflector.

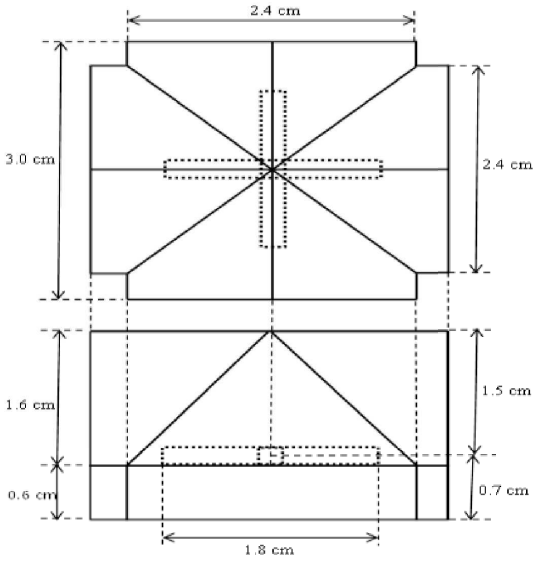

Figure 5. Construction and dimensions of the transmitting element: two crossed dipoles enclosed by a metallic reflector.

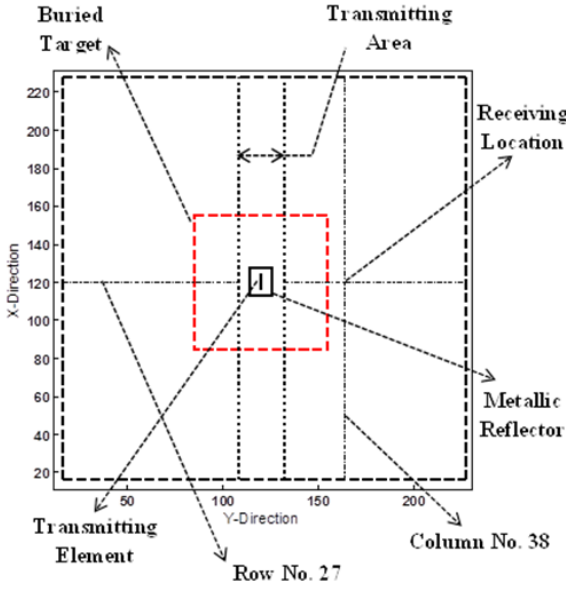

Figure 6. Top view description of the computational domain.

arranged in the plane just above the ground surface, a two-dimensional image can be constructed from the scattering parameter data between transmitting and receiving antenna elements.

4. RESULTS AND DISCUSSION

The results are obtained when a Gaussian pulse source is applied at the dipole center of the transmitting antenna of a polarimetric GPR sensor placed at a height of 0.6 cm over empty ground and at the same height over the same ground containing a buried target. The cell size is $2 \times 2 \times 2\,\text{mm}^3$. Seven-cell PML is used to satisfy absorbing boundary condition. A GPR antenna array of 54×54 crossed-dipole antenna elements is used, and each element is composed of an x-oriented dipole crossed with another y-oriented dipole. The dimensions of the antenna array are 42.4 cm $\times$ 42.4 cm, and the length of the single dipole element is 6 mm. Two types of targets are considered. The first one is a dielectric type described as "plexiglass block target" and has the following properties: $\varepsilon_r = 2.6$, $\mu_r = 1.0$, and $\sigma = 0.0\,\text{S/m}$; these properties are similar to those of nonmetallic landmines, which generally have plastic exteriors (ε_r near 3) and TNT ($\varepsilon_r \approx 2.89$) as the primary filler. The second one is a metallic type has the following properties: $\varepsilon_r = 1.0$, $\mu_r = 1.0$, and $\sigma = 10^7\,\text{S/m}$; these properties are similar to those of the metallic land mines. All targets are cubic-shaped block and have the dimensions $14 \times 14 \times 7.2$ cm and buried at 10 cm under the ground surface. For the detection process, only the xx channel data is used, and the received signal is measured at receiving antenna placed in the row number 27 and column number 38 in the sensor array as shown in Fig. 6.

4.1. Detecting and Imaging a Dielectric Target Buried in Realistic Dispersive Soil

Figure 7 shows the coupling between the transmitting and receiving antennas when the polarimetric sensor is placed over empty Puerto Rico clay loams with 10% moisture content and when it is placed over the same soil with plexiglass block target of dimension $14 \times 14 \times 7.2$ cm buried at a depth of 10 cm. As shown in this figure, there is an increase in coupling between antennas due to the existence of the buried target. The frequency band within which a plexiglass block target is most detectable when buried in such a soil is 4–10 GHz, with maximum detectability at 8 GHz.

It is clear in the figure that the coupling difference values range from 4 dB to 22 dB in the frequency band 2–4 GHz and range from 17 dB to 23.5 dB in the band 4–10 GHz. Hence, the dispersion effect of

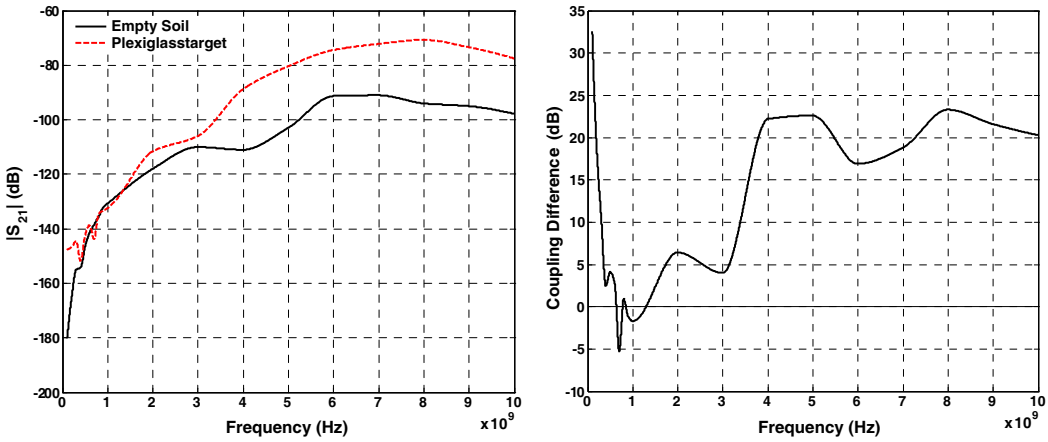

Figure 7. Coupling between the sensor antennas when it is placed over an empty Puerto Rico clay loams soil (no target) and when placed over the same soil with a plexiglass block buried at a depth of 10 cm.

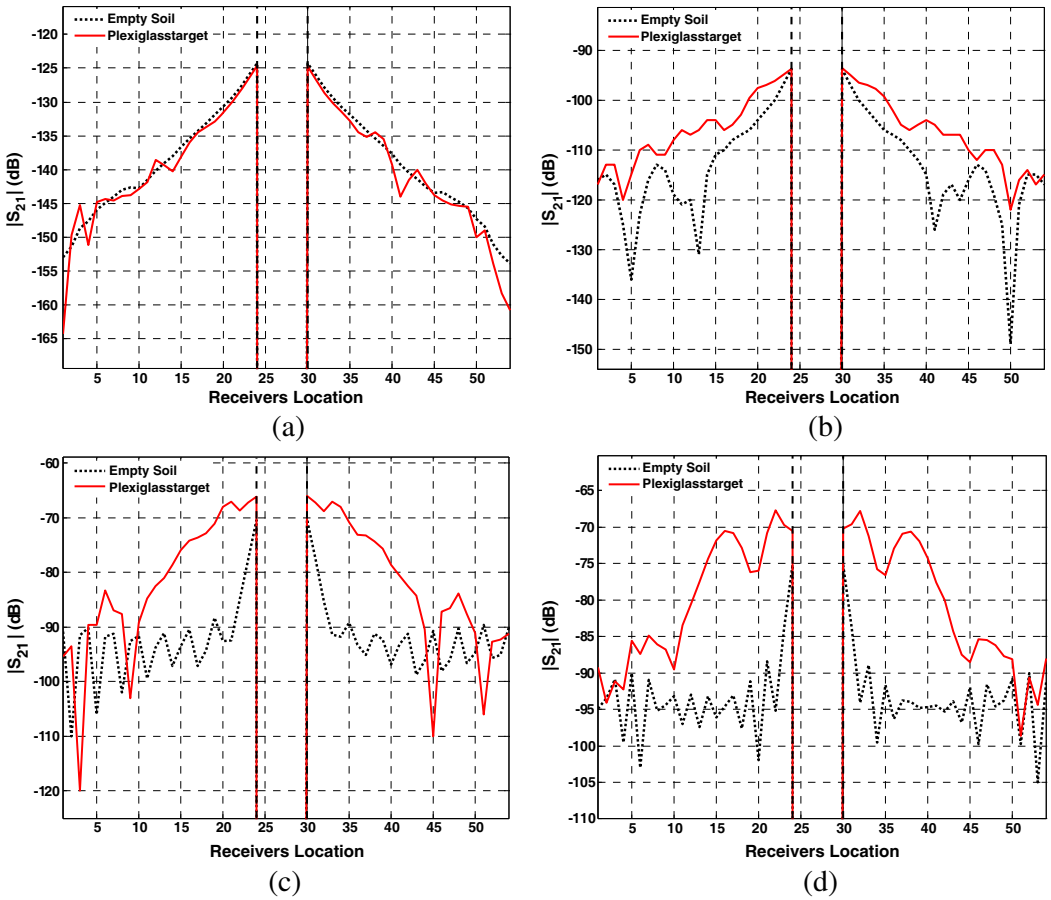

Figure 8. Coupling between the sensor antennas when it is placed over an empty Puerto Rico clay loams soil (no target) and when placed over the same soil with a plexiglass block buried at a depth of 10 cm, at different frequencies. (a) 800 MHz. (b) 3 GHz. (c) 6 GHz. (d) 8 GHz.

this soil on the plexiglass target detectability does not appear clearly at frequencies above 4 GHz.

Figure 8 shows the antenna coupling dependence on the receiver location when the polarimetric sensor is placed over empty Puerto Rico clay loams with 10% moisture content and when it is placed

over the same soil with plexiglass block target of dimension $14 \times 14 \times 7.2$ cm buried at a depth of 10 cm at different frequencies. The dashed line in these figures indicates the region in which the transmitting antenna element is placed, and there are no receiving elements. At 800 MHz, the sensor cannot detect this target at all receiving elements locations due to the numerical noise as shown in Fig. 8(a). In Fig. 8(b), at 3 GHz, the sensor can detect this target at most receiving element except at the farther receivers due to low level of the reflected signal from target, and at the receivers adjacent to the transmitting area due to the higher level of the direct coupling signal compared with the reflected signal from the target. At 6 GHz the sensor can detect this target at most receiving elements as in Fig. 8(c). At 8 GHz the sensor can detect this target at all receiving elements, except at the farther receivers on the two sides as in Fig. 8(d).

It is clear from these figures that the detection capability of this target, when buried in the Puerto Rico clay loams soil, depends on the sensor operating frequency and location of the receiving element in antenna array.

The GPR images are obtained for a plexiglass block buried at a depth of about 10 cm below the surface of Puerto Rico clay loams soil using the data collected from the polarimetric GPR sensor. For visualizing the two-dimensional GPR data, the absolute value of the scattering parameters for the xx-channel are shown in Fig. 9 at different frequencies. It is shown that at the frequencies near the soil relaxation frequency it is difficult to have a good image for this target because the high losses value makes the sensor not capable to image the target when buried in such soil at these frequencies.

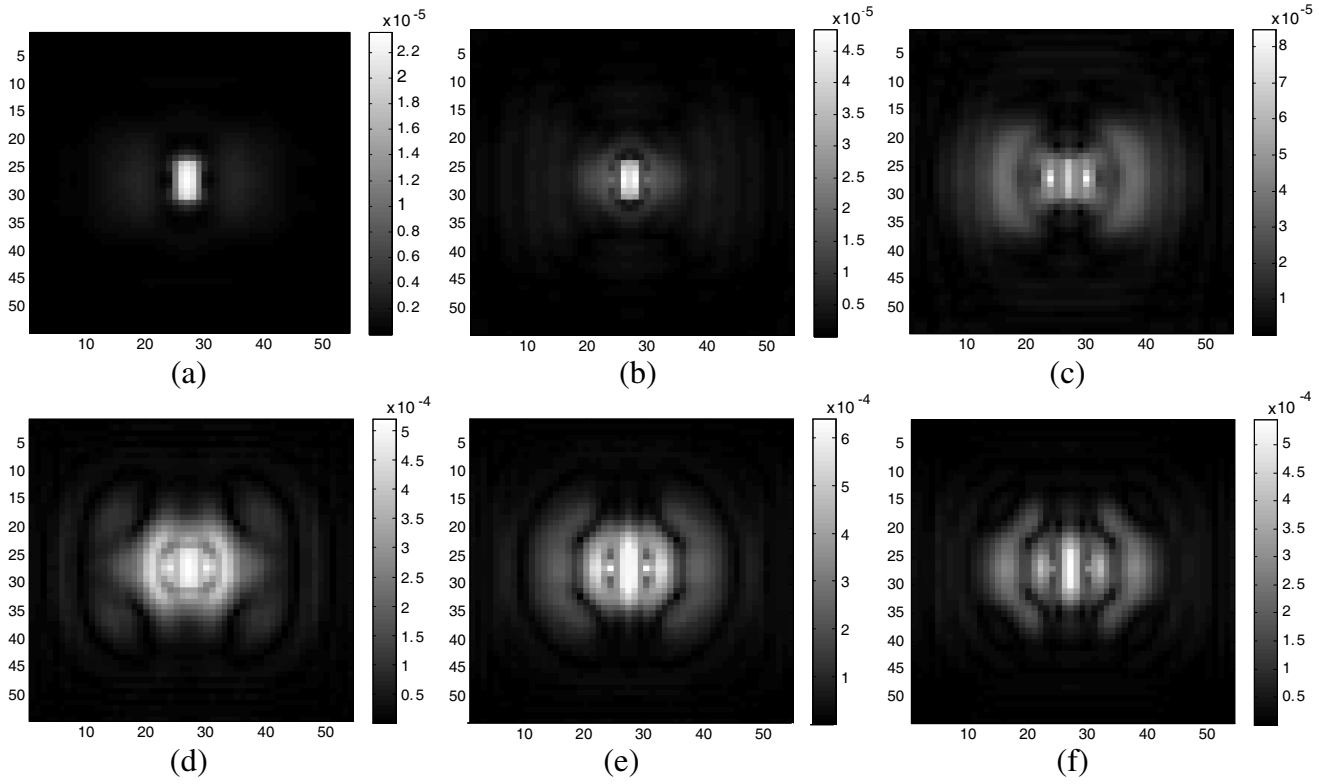

Figure 9. The XX-channel image for Plexiglass block buried at 10 cm depth below the surface of Puerto Rico clay loams soil; at different frequencies. (a) 2 GHz. (b) 3 GHz. (c) 4 GHz. (d) 6 GHz. (e) 7 GHz. (f) 8 GHz.

4.1.1. Shape Extraction and Recognition for a Dielectric Target Buried in Realistic Dispersive Soil

Figure 10 shows the GPR images for a plexiglass block buried at a depth of about 10 cm below the ground surface at 8 GHz. These images are extracted from the polarimetric data as described in [8, 9]. For visualizing the two-dimensional GPR data, the absolute values of the scattering parameters are

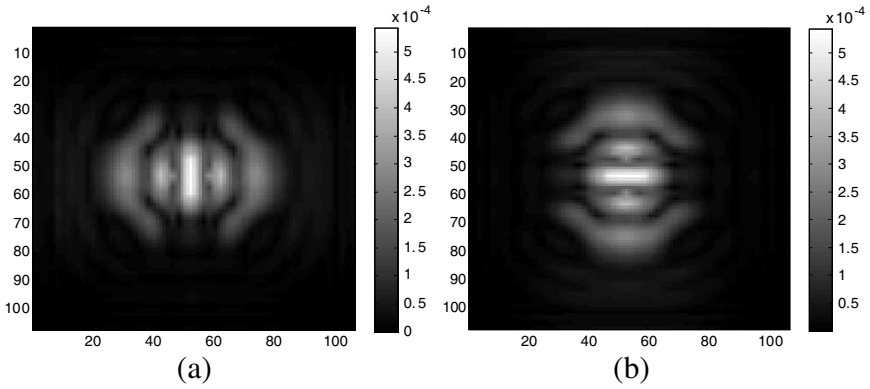

Figure 10. The XX-channel and the YY-channel images for a plexiglass block buried in Puerto Rico clay loams soil; at 8 GHz. (a) Image from XX-channel. (b) Image from YY-channel.

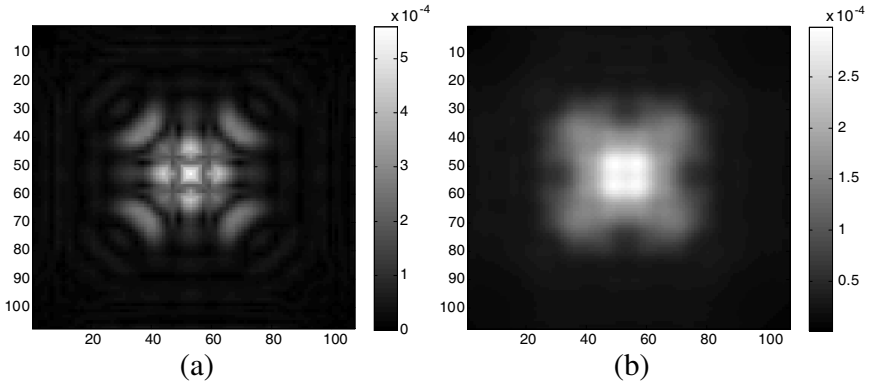

Figure 11. The plexiglass block image constructed from the XX-channel and the YY-channel images when buried in Puerto Rico clay loams soil; at 8 GHz. (a) Constructed image. (b) Smoothed image.

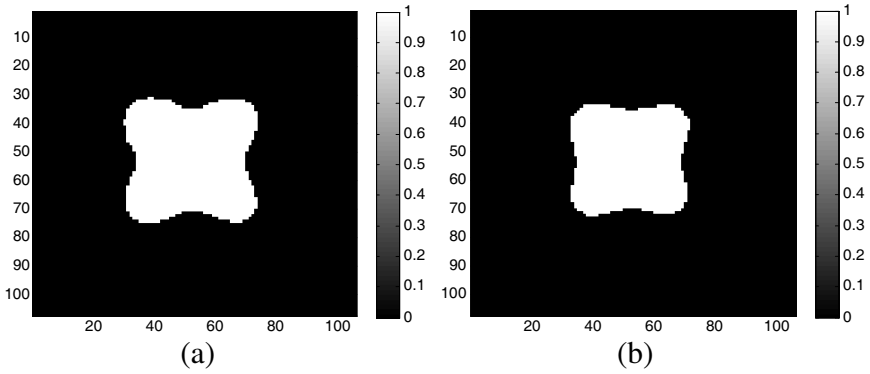

Figure 12. The recovered shape for a plexiglass block buried in Puerto Rico clay loams soil; at 8 GHz. (a) Recovered shape. (b) Smoothed shape.

shown in Fig. 10(a) for the XX-channel and Fig. 10(b) for the YY-channel. The constructed image shown in Fig. 11(a) and a smoothed image shown in Fig. 11(b).

The procedure described in [8, 9] for buried object shape (BOS) extraction is applied without using the smoothing shape filter (SSF), and the binary image is then obtained and presented in Fig. 12(a). The SSF is then applied to get the smoothed shape of the buried object shown in Fig. 12(b). The procedure described in [8, 9] to extract the shape boundary curve (SBC) is applied, and the extracted curve presented in Fig. 13. For target shape recognition, the reference target shape is shown in Fig. 14, and the retrieved SBCs are compared with their centroids coincident with each other. The relative mismatch error between the two boundary-curves is then calculated. In this case, the squared mismatch

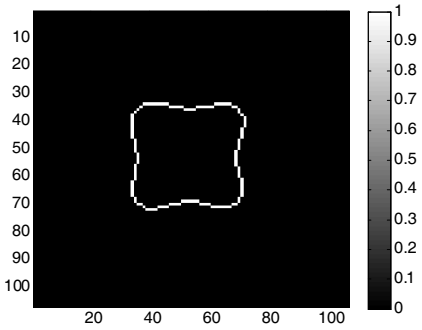

Figure 13. The retrieved boundary shape curve for a plexiglass block buried in Puerto Rico clay loams soil; at 8 GHz.

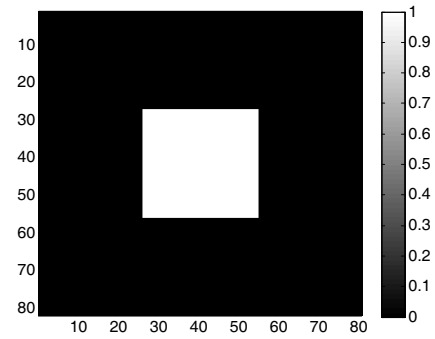

Figure 14. The reference shape curve for a buried cuboid block.

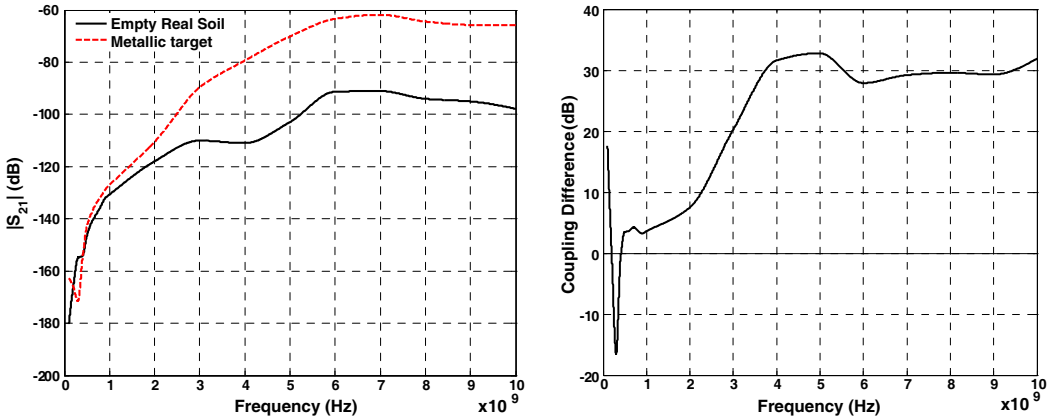

Figure 15. Coupling between the sensor antennas when it is placed over an empty Puerto Rico clay loams soil (no target) and when placed over the same soil with a metallic block buried at a depth of 10 cm.

error is 0.58%. Such a small value of the squared mismatch error means that the target is recognized at 8 GHz.

4.2. Detecting and Imaging a Metallic Target Buried in Realistic Dispersive Soil

Figure 15 shows the coupling between the transmitting and receiving antennas when the polarimetric sensor is placed over empty Puerto Rico clay loams with 10% moisture content and when it is placed over the same soil with metallic block target of dimension $14 \times 14 \times 7.2$ cm buried at a depth of 10 cm. As shown in this figure, there is an increase in coupling between antennas due to the existence of the buried target. The frequency band within which a metallic block target is most detectable when buried in such a soil is 3–10 GHz, with maximum detectability at 5 GHz.

It is clear in the figure that the coupling difference values range from 7.5 dB to 31.5 dB in the frequency band 2–4 GHz and range from 28 dB to 33 dB in the band 4–10 GHz. Hence, the dispersion effect of this soil on the metallic target detectability does not appear clearly at frequencies above 4 GHz.

Figure 16 shows the antenna coupling dependence on the receiver location when the polarimetric sensor is placed over empty Puerto Rico clay loams with 10% moisture content and when it is placed over the same soil with metallic block target of dimension $14 \times 14 \times 7.2$ cm buried at a depth of 10 cm at different frequencies. The dashed line in these figures indicates the region in which the transmitting antenna element was placed and there is no receiving elements. At 800 MHz, the sensor cannot detect this target at all receiving elements locations due to the numerical noise as shown in Fig. 16(a). At 3 GHz, 6 GHz, and 8 GHz, the sensor can detect this target at all receiving elements, except at the farther receivers on the two sides due to low level of the reflected signal from target as in Fig. 16(b),

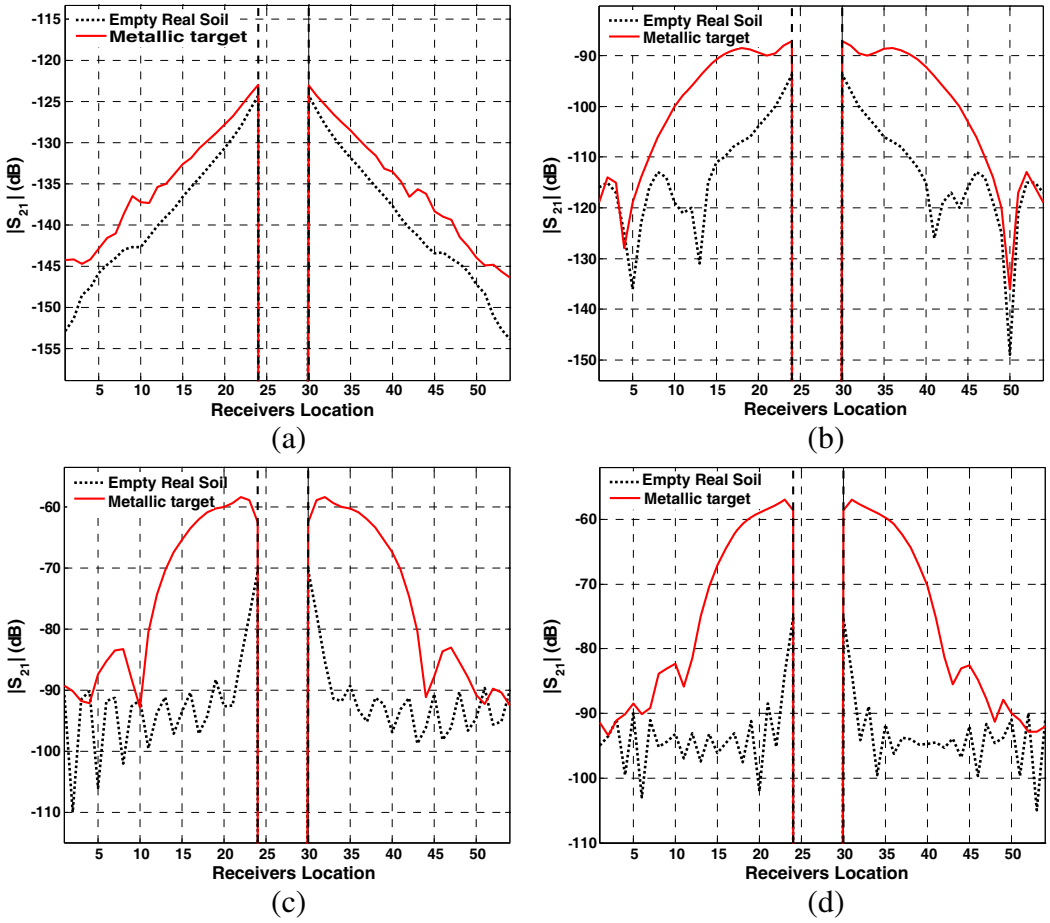

Figure 16. Coupling between the sensor antennas when it is placed over an empty Puerto Rico clay loams soil (no target) and when placed over the same soil with a metallic block buried at a depth of 10 cm, at different frequencies. (a) 800 MHz. (b) 3 GHz. (c) 6 GHz. (d) 8 GHz.

Fig. 16(c), and Fig. 16(d), respectively.

It is clear from these figures that the metallic target can be easily detected when buried in this dispersive soil due to the contrast between the electrical properties of target and soil at all frequencies except at the frequencies near to the soil relaxation frequency due to the higher losses level. The detection capability of this target depends on the location of the receiving element in antenna array.

The GPR images are obtained for a metallic block buried at a depth of about 10 cm below the surface below the surface of Puerto Rico clay loams soil using the data collected from the polarimetric GPR sensor. For visualizing the two-dimensional GPR data, the absolute value of the scattering parameters for the xx-channel are shown in Fig. 17 at different frequencies. It is shown that at the frequencies near the soil relaxation frequency it is difficult to have a good image for this target because the high losses value makes the sensor not capable to image the target when buried in such soil at these frequencies.

4.2.1. Shape Extraction and Recognition for a Metallic Target Buried in Realistic Dispersive Soil

Figure 18 shows the GPR images for a metallic block buried at a depth of about 10 cm below the ground surface at 6 GHz. These images are extracted from the polarimetric data. For visualizing the two-dimensional GPR data, the absolute values of the scattering parameters are shown in Fig. 18(a) for the XX-channel and Fig. 18(b) for the YY-channel. The constructed image is shown in Fig. 19(a) and a smoothed image shown in Fig. 19(b).

The procedure described for BOS extraction is applied without using the SSF and the binary image described is then obtained and presented in Fig. 20(a). The SSF is then applied to get the smoothed

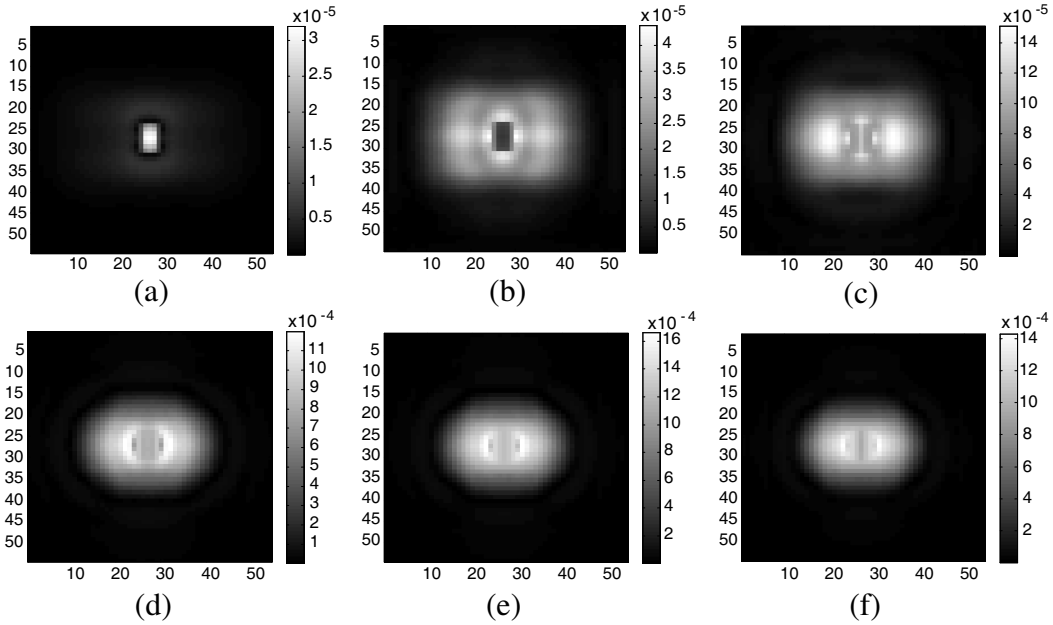

Figure 17. The XX-channel image for metallic block buried at 10 cm depth below the surface of Puerto Rico clay loams soil; at different frequencies. (a) 2 GHz. (b) 3 GHz. (c) 4 GHz. (d) 6 GHz. (e) 7 GHz. (f) 8 GHz.

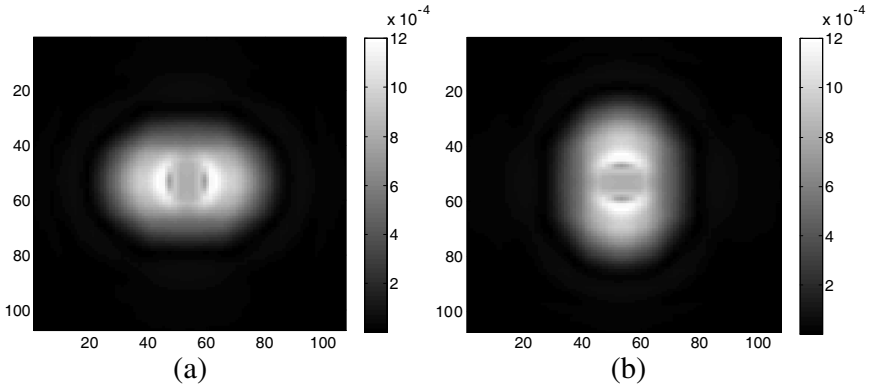

Figure 18. The XX-channel and the YY-channel images for a metallic block buried in Puerto Rico clay loams soil; at 6 GHz. (a) Image from XX-channel. (b) Image from YY-channel.

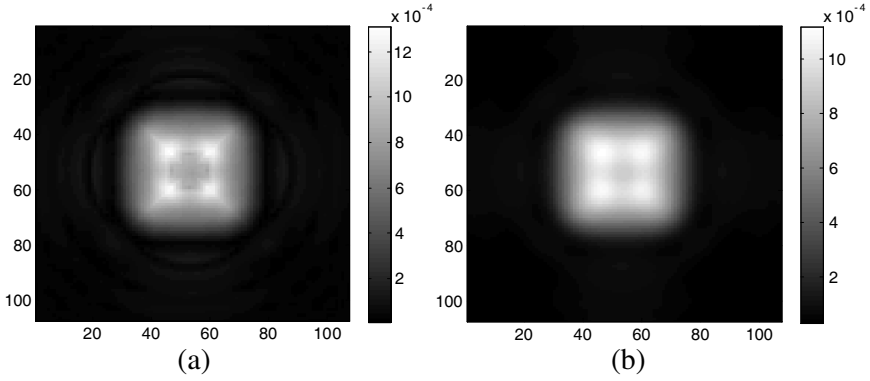

Figure 19. The metallic block image constructed from the XX-channel and the YY-channel images when buried in Puerto Rico clay loams soil; at 6 GHz. (a) Constructed image. (b) Smoothed image.

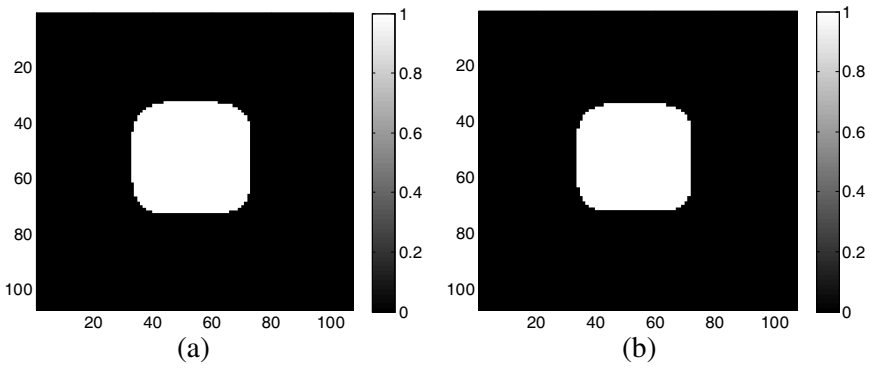

Figure 20. The recovered shape for a metallic block buried in Puerto Rico clay loams soil; at 6 GHz. (a) Recovered shape. (b) Smoothed shape.

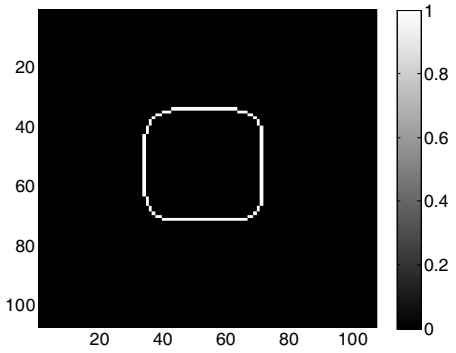

Figure 21. The retrieved boundary shape curve for a metallic block buried in Puerto Rico clay loams soil; at 6 GHz.

shape of the buried object shown in Fig. 20(b). The procedure described to extract the SBC is applied, and the extracted boundary curve is presented in Fig. 21. For target shape recognition, the reference target shape is shown in Fig. 14, and the retrieved SBCs are compared with their centroids coincident with each other. The relative mismatch error between the two boundary-curves is then calculated. In this case, the squared mismatch error is 0.36%. Such a small value of the squared mismatch error means that the target is recognized.

4.3. Detecting and Imaging a Dielectric Block Buried in Hypothetical Dispersive Soil

Figure 22 shows the coupling between the transmitting and receiving antennas when the polarimetric sensor is placed over empty hypothetical dispersive soil and when it is placed over the same soil with plexiglass block target of dimension $14 \times 14 \times 7.2$ cm buried at a depth of 10 cm. This coupling measured between the transmitting antenna and a receiving antenna is placed in the row number 27 and column number 38 in the sensor array. As shown in this figure, the frequency band within which a plexiglass block target is most detectable when buried in such a soil is 2–9 GHz, with maximum detectability at 6 GHz.

It is clear in the figure that the coupling difference values range from 1 dB to 27 dB in the band 4–10 GHz. Hence, the dispersion effect of this soil on the plexiglass target detectability is clear at frequencies above 4 GHz.

Figure 23 shows the dependence of the antenna coupling on the receiver location when the polarimetric sensor is placed over empty hypothetical dispersive soil and when it is placed over the same soil with plexiglass block target of dimension $14 \times 14 \times 7.2$ cm buried at a depth of 10 cm at different frequencies. The dashed line in these figures indicates the region in which the transmitting antenna element is placed, and there are no receiving elements. At 800 MHz, the sensor cannot detect

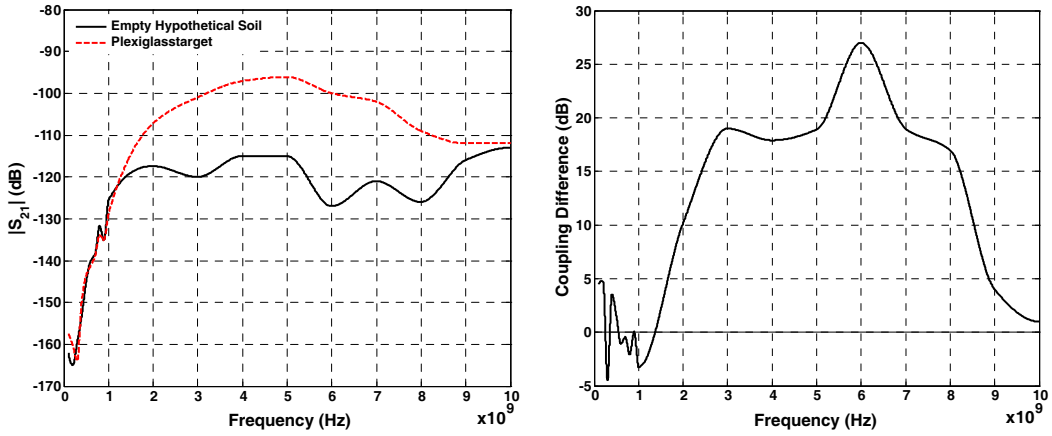

Figure 22. Coupling between the sensor antennas when it is placed over an empty hypothetical dispersive soil (no target) and when placed over the same soil with a plexiglass block buried at a depth of 10 cm.

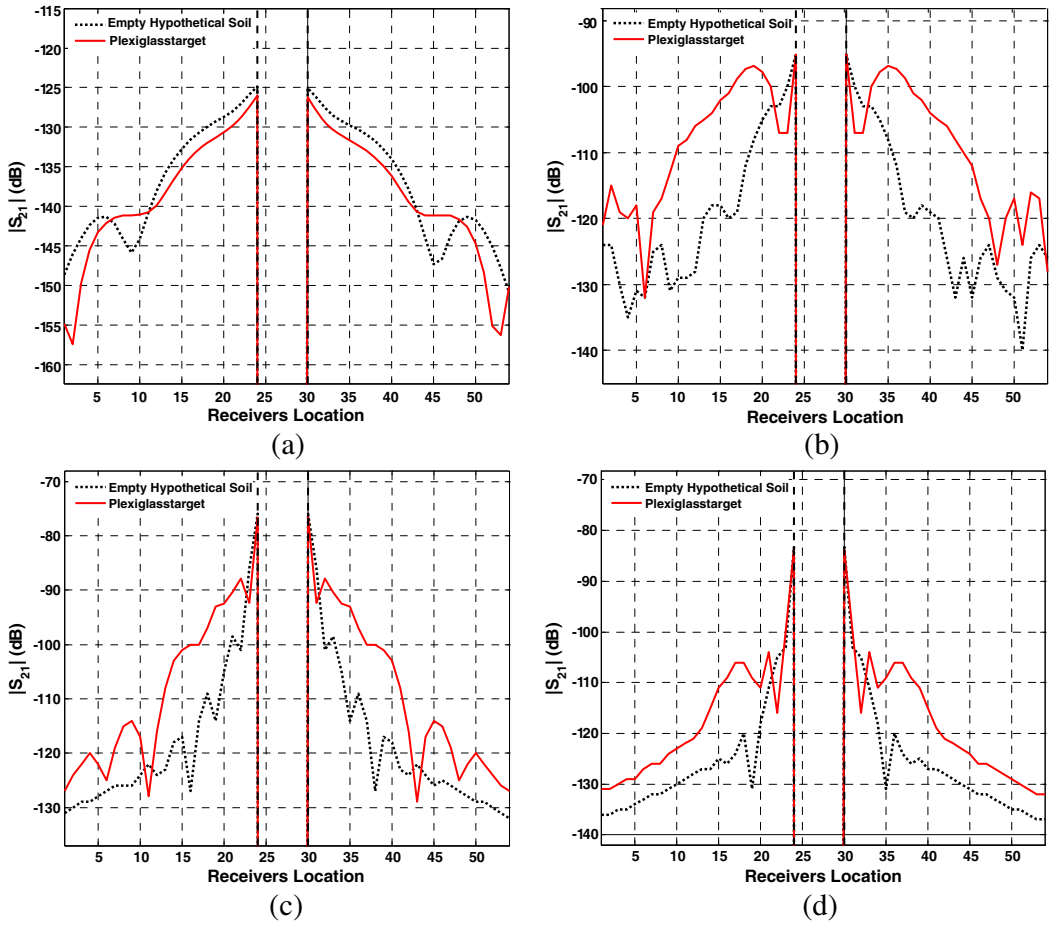

Figure 23. Coupling between the sensor antennas when it is placed over an empty hypothetical dispersive soil (no target) and when placed over the same soil with a plexiglass block buried at a depth of 10 cm, at different frequencies. (a) 800 MHz. (b) 3 GHz. (c) 6 GHz. (d) 8 GHz.

this target at all receiving elements locations due to the numerical noise as shown in Fig. 23(a). In Fig. 23(b), at 3 GHz, the sensor can detect this target at most receiving elements except at at the receivers adjacent to the transmitting area due to the higher level of the direct coupling signal than the reflected signal from the target. At 6 GHz, the sensor can detect this target at most receiving elements depending on their location in the antenna array except at the receivers adjacent to the transmitting area due to the higher level of the direct coupling signal than the reflected signal from the target as in Fig. 23(c). At 8 GHz, the sensor can detect this target only at the receiving element near the transmitting area due to the higher level of soil losses at this frequency, except at the receivers adjacent to the transmitting area as in Fig. 23(d).

It is clear from these figures that the detection capability of the plexiglass target when buried in that hypothetical soil depends on the sensor operating frequency, the relaxation frequency at which the maximum loss occurs, and the location of the receiving element in antenna array.

The GPR images are obtained for a plexiglass block buried at a depth of about 10 cm below the surface of hypothetical dispersive soil using the data collected from the polarimetric GPR sensor. For visualizing the two-dimensional GPR data, the absolute values of the scattering parameters for the xx-channel are shown in Fig. 24 at different frequencies. The target cannot image clearly at the frequencies near the relaxation frequency, 7.2 GHz, due to the high losses of this soil.

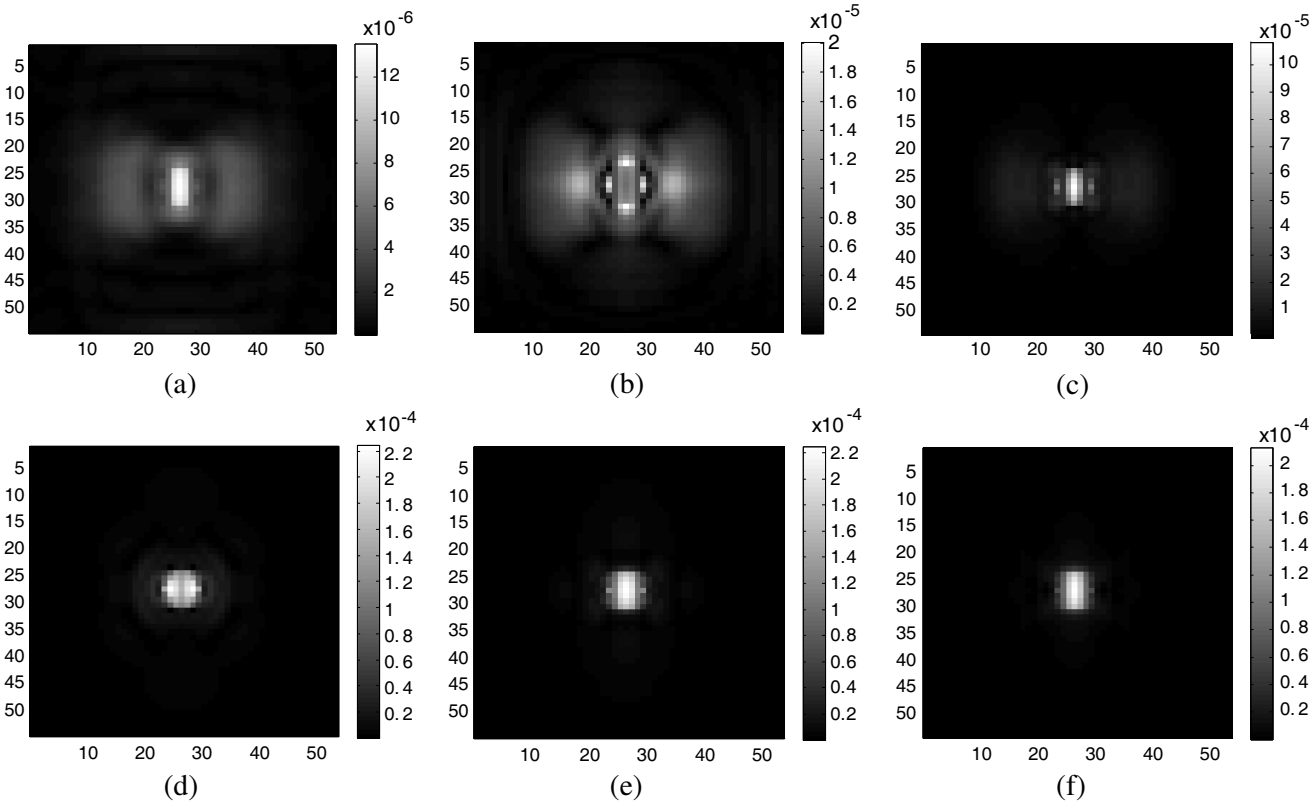

Figure 24. The XX-channel image for Plexiglass block buried at 10 cm depth below the surface of hypothetical dispersive soil; at different frequencies. (a) 2 GHz. (b) 3 GHz. (c) 4 GHz. (d) 6 GHz. (e) 7 GHz. (f) 8 GHz.

4.3.1. Shape Extraction and Recognition for a Dielectric Block Buried in Hypothetical Dispersive Soil

Figure 25 shows the GPR images for a plexiglass block buried at a depth of about 10 cm below the ground surface at 6 GHz. These images are extracted from the polarimetric data. For visualizing the two-dimensional GPR data, the absolute values of the scattering parameters are shown in Fig. 25(a) for the XX-channel and Fig. 25(b) for the YY-channel. The constructed image is shown in Fig. 26(a)

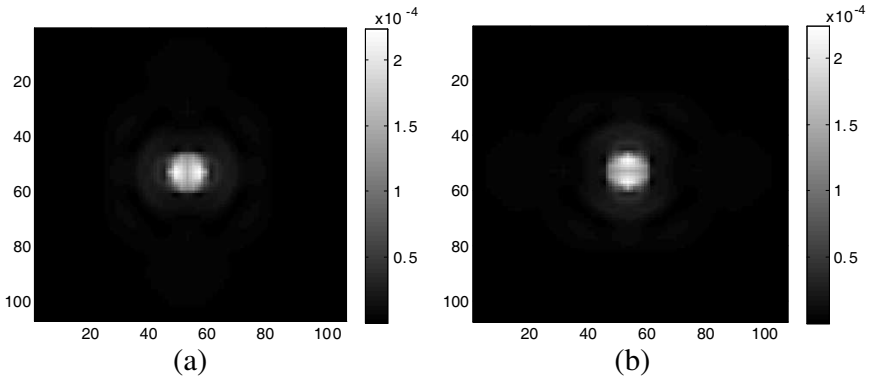

Figure 25. The XX-channel and the YY-channel images for a plexiglass block buried in hypothetical dispersive soil; at 6 GHz. (a) Image from XX-channel. (b) Image from YY-channel.

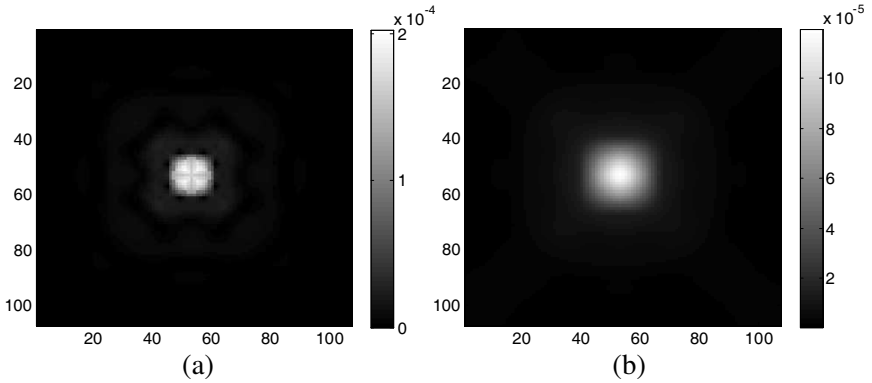

Figure 26. The plexiglass block image constructed from the XX-channel and the YY-channel images when buried in hypothetical dispersive soil; at 6 GHz. (a) Constructed image. (b) Smoothed image.

and a smoothed image shown in Fig. 26(b).

The procedure described for BOS extraction is applied without using the SSF, and the binary image is then obtained and presented in Fig. 27(a). The SSF is then applied to get the smoothed shape of the buried object shown in Fig. 27(b). The procedure described to extract the SBC is applied and the boundary curve presented in Fig. 28. For target shape recognition, the reference target shape is shown in Fig. 14, and the retrieved SBCs are compared with their centroids coincident with each other. The relative mismatch error between the two boundary-curves is then calculated. In this case, the squared mismatch error is 0.81%. Such a small value of the squared mismatch error means that the target is recognized.

4.4. Detecting and Imaging a Metallic Block Buried in Hypothetical Dispersive Soil

Figure 29 shows the coupling between the transmitting and receiving antennas when the polarimetric sensor is placed over empty hypothetical dispersive soil and when it is placed over the same soil with metallic block target of dimension $14 \times 14 \times 7.2$ cm buried at a depth of 10 cm. This coupling measured between the transmitting antenna and a receiving antenna placed in the row number 27 and column number 43 in the sensor array. As shown in this figure, there is a considerable increase in the coupling over the frequency band 2–8 GHz due to the existence of the metallic target. Also, this target has maximum detectability at 6 GHz.

Figure 30 shows the dependence of antenna coupling on the receiver location when the polarimetric sensor is placed over empty hypothetical dispersive soil and when it is placed over the same soil with metallic block target of dimension $14 \times 14 \times 7.2$ cm buried at a depth of 10 cm at different frequencies.

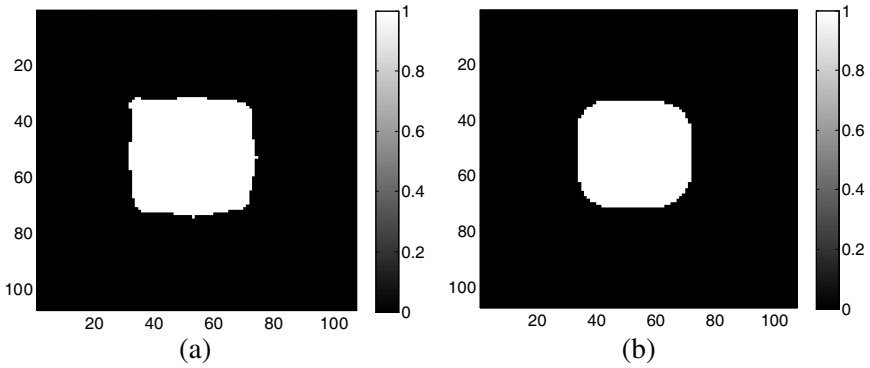

Figure 27. The recovered shape for a plexiglass block buried in hypothetical dispersive soil; at 6 GHz. (a) Recovered shape. (b) Smoothed shape.

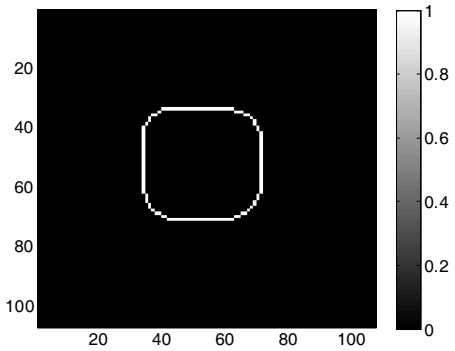

Figure 28. The retrieved boundary shape curve for a plexiglass block buried in hypothetical dispersive soil; at 6 GHz.

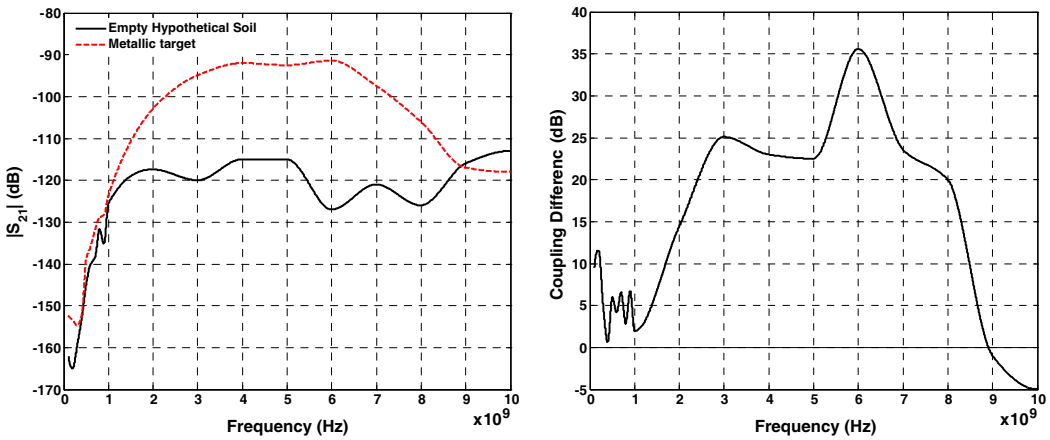

Figure 29. Coupling between the sensor antennas when it is placed over an empty hypothetical dispersive soil (no target) and when placed over the same soil with a metallic block buried at a depth of 10 cm.

The dashed line in these figures indicates the region in which the transmitting antenna element was placed and there is no receiving elements. At 800 MHz, the sensor cannot detect this target at all receiving elements locations due to the numerical noise as shown in Fig. 30(a). At 3 GHz and 6 GHz, the sensor can detect this target at all receiving elements with level depending on their location in the sensor array as in Figs. 30(b) and 30(c), respectively. At 8 GHz, the sensor can detect this target only

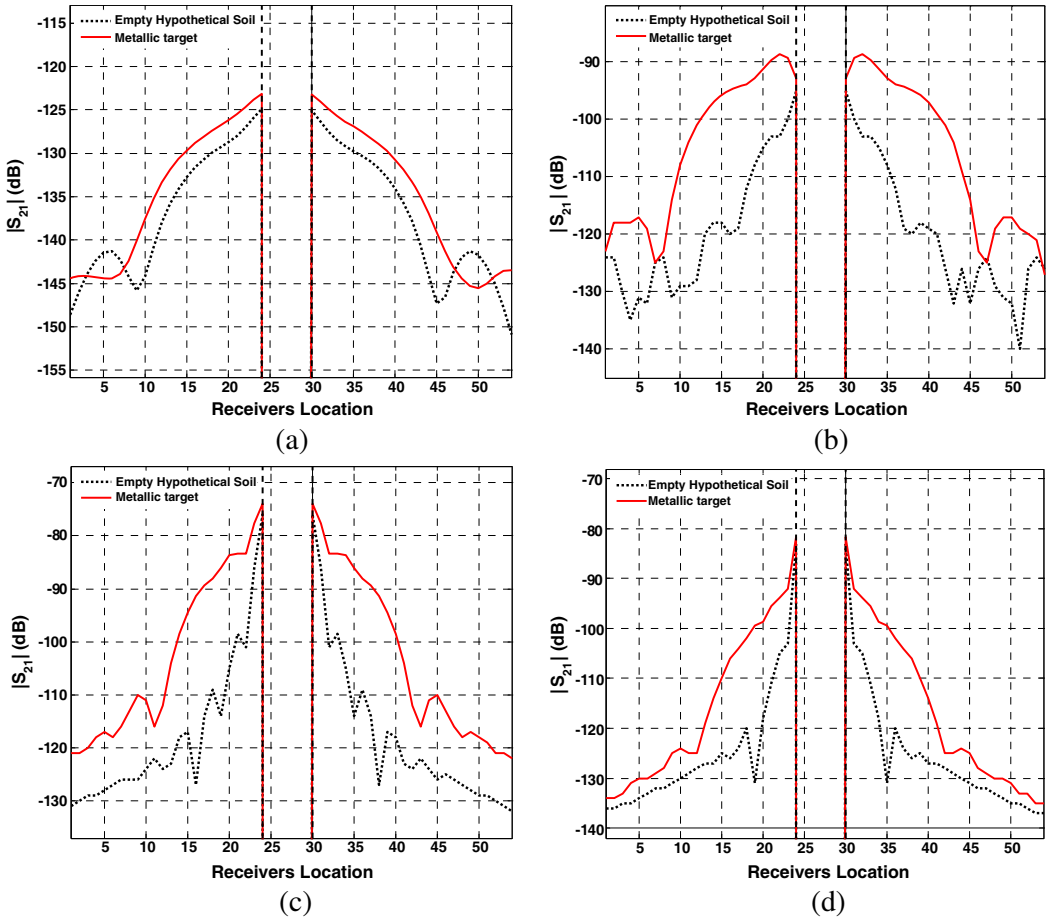

Figure 30. Coupling between the sensor antennas when it is placed over an empty hypothetical dispersive soil (no target) and when placed over the same soil with a metallic block buried at a depth of 10 cm, at different frequencies. (a) 800 MHz. (b) 3 GHz. (c) 6 GHz. (d) 8 GHz.

at the receiving element near from the transmitting area due to the higher level of soil losses at this frequency, except at the receivers adjacent to the transmitting area as in Fig. 30(d).

It is clear from these figures that the metallic target can be easily detected when buried in the hypothetical dispersive soil due to the contrast between the electrical properties of target and soil at all frequencies except at the frequencies near the soil relaxation frequency due to the higher losses level. The detection capability of this target depends on the location of the receiving element in antenna array.

The GPR images are obtained for a metallic block buried at a depth about 10 cm below the surface of hypothetical dispersive soil using the data collected from the polarimetric GPR sensor. For visualizing the two-dimensional GPR data, the absolute values of the scattering parameters for the xx-channel are shown in Fig. 31 at different frequencies. It is shown that at the frequencies near the soil relaxation frequency it is difficult to have a good image for this target because of the high losses value that makes the sensor not capable to image the target when buried in such soil at these frequencies.

4.4.1. Shape Extraction and Recognition for a Metallic Block Buried in Hypothetical Dispersive Soil

Figure 32 shows the GPR images for a metallic block buried at a depth of about 10 cm below the ground surface at 6 GHz. These images are extracted from the polarimetric data. For visualizing the two-dimensional GPR data, the absolute values of the scattering parameters are shown in Fig. 32(a) for the XX-channel and Fig. 32(b) for the YY-channel. The constructed image is shown in Fig. 33(a) and a smoothed image shown in Fig. 33(b).

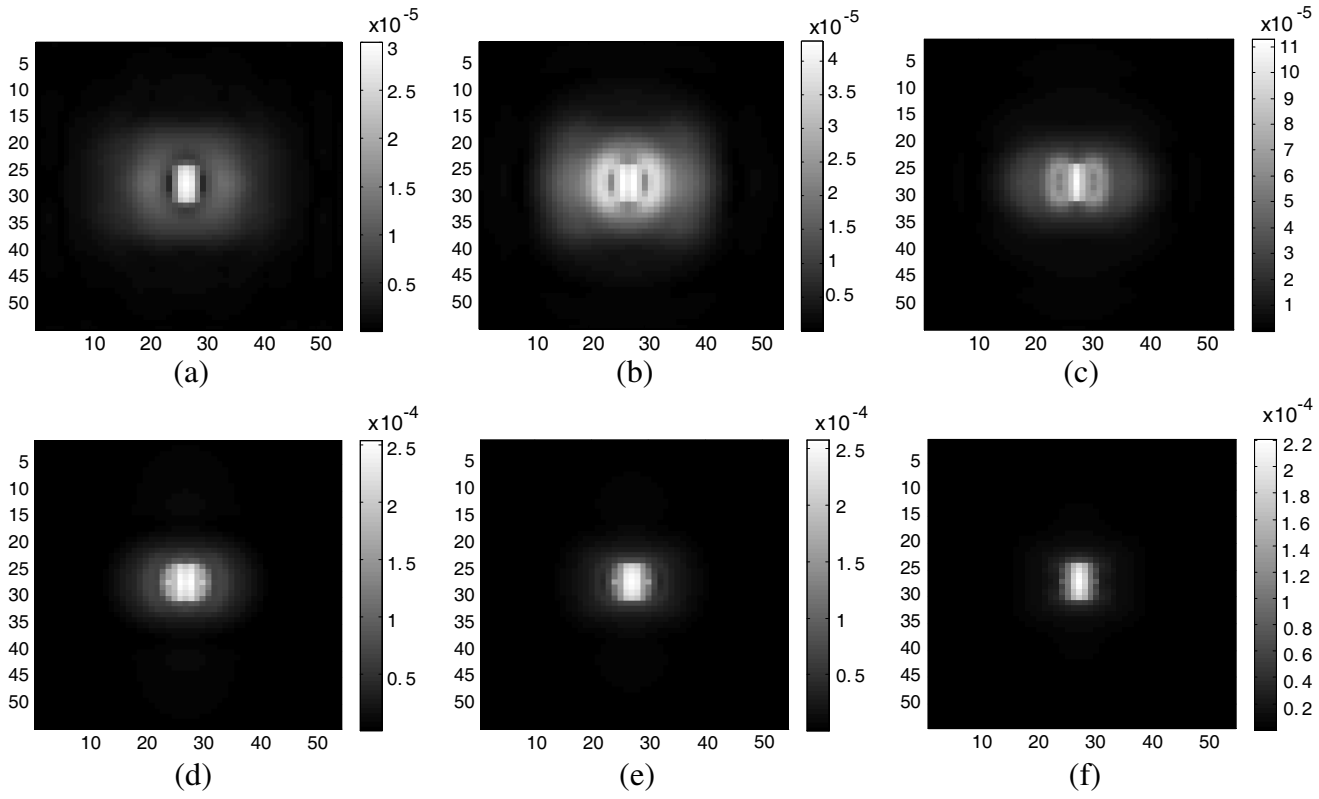

Figure 31. The XX-channel image for metallic block buried at 10 cm depth below the surface of hypothetical dispersive soil; at different frequencies. (a) 2 GHz. (b) 3 GHz. (c) 4 GHz. (d) 6 GHz. (e) 7 GHz. (f) 8 GHz.

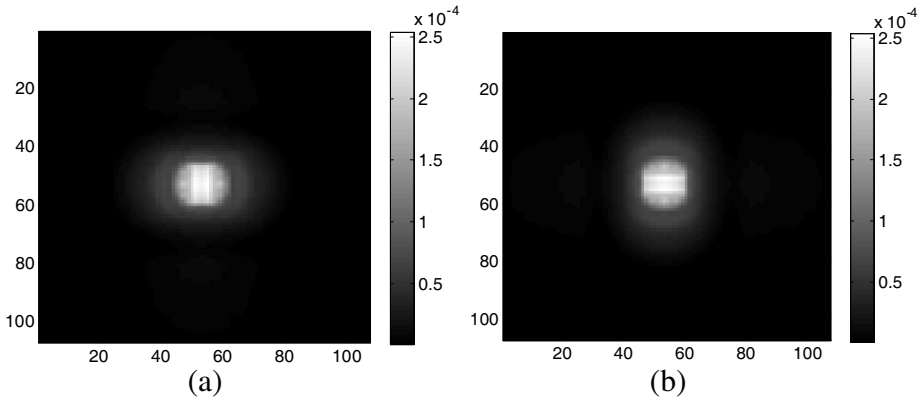

Figure 32. The XX-channel and the YY-channel images for a metallic block buried in hypothetical dispersive soil; at 6 GHz. (a) Image from XX-channel. (b) Image from YY-channel.

The procedure described for BOS extraction is applied without using the SSF, and the binary image is then obtained and presented in Fig. 34(a). The SSF is then applied to get the smoothed shape of the buried object shown in Fig. 34(b). The procedure described to extract the SBC is applied and then the extracted curve presented in Fig. 35. For target shape recognition, the reference target shape shown in Fig. 14, and the retrieved SBCs are compared with their centroids coincident with each other. The relative mismatch error between the two boundary-curves is then calculated. In this case, the squared mismatch error is 1.44%, and the target may be recognized.

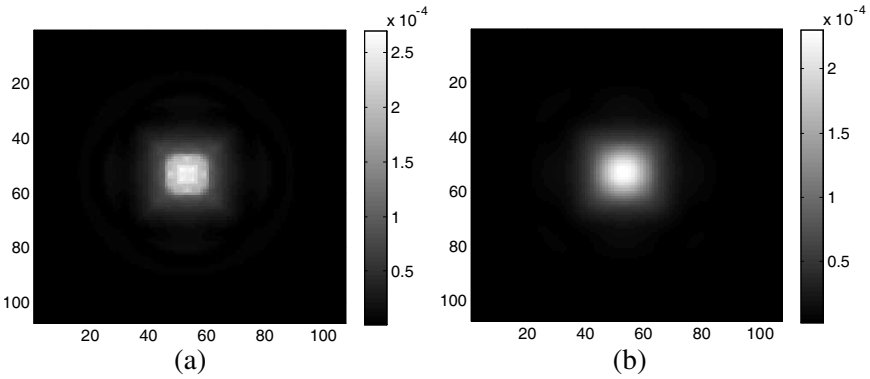

Figure 33. The metallic block image constructed from the XX-channel and the YY-channel images when buried in hypothetical dispersive soil; at 6 GHz. (a) Constructed image. (b) Smoothed image.

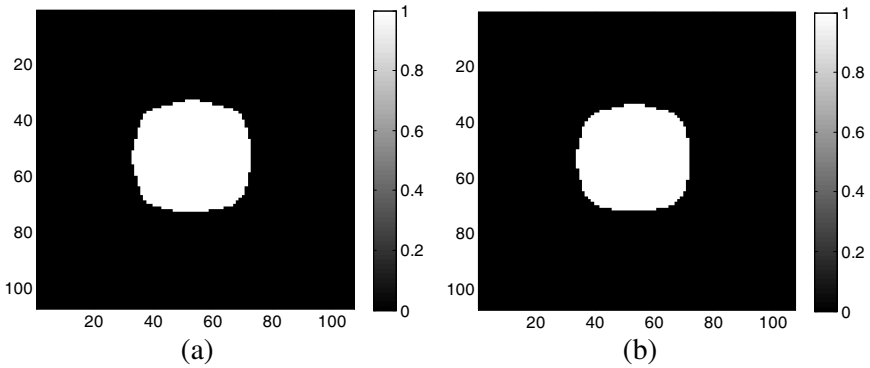

Figure 34. The recovered shape for a metallic block buried in hypothetical dispersive soil; at 6 GHz. (a) Recovered shape. (b) Smoothed shape.

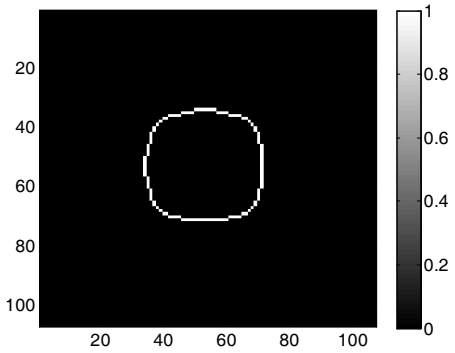

Figure 35. The retrieved boundary shape curve for a metallic block buried in hypothetical dispersive soil; at 6 GHz.

5. CONCLUSION

The capability of the polarimetric GPR sensor to detect buried targets in dispersive soil is examined using a Gaussian pulse excitation applied at the feed point of the sensor transmitting antenna. The increase in the electromagnetic coupling between the transmitting and receiving antennas of the sensor due to the presence of the target is used as a measure of the system capability.

Two dispersive soil models are simulated to demonstrate the dispersion effects on the target detection capability. The first one is real soil with relaxation frequency at 700 MHz, hence the dispersion effects appear at low frequencies, at this frequency the losses have the maximum value, while the second one is a hypothetical model designed with a relaxation frequency at 7.2 GHz to obtain the dispersion

effects at high frequencies.

The target detection capability is shown to be dependent on the receiving element location. At the receiving elements adjacent to the transmitting area, the level of the reflected signal from target is small compared with that of the direct coupling signal, and also, at the farther receivers the reflected signal from target is very low.

It is shown that at frequencies far from the relaxation frequency, the existence of target results in a considerable increase in the antennas coupling. On the other hand, at the frequencies around the relaxation frequency, the existence of target does not necessarily result in a significant increase in the antennas coupling. At these frequencies, the existence of target may result in a little increase in the antennas coupling at a certain frequency whereas results in a decrease in the coupling at another frequency.

It is shown that at the relaxation frequency the soil losses has the maximum value. Therefore, around the relaxation frequency it is very difficult to have a good image even with targets having high contrast with the background soil. However, the target shape can be extracted and recognized at the frequencies near the relaxation frequency.

REFERENCES

1. Taflove, A. and S. C. Hagness, *Computational Electrodynamics: The Finite-difference Time-domain Method*, Artech House, 2005.
2. Taflove, A., *Advances in Computational Electrodynamics: The Finite-difference Time-domain Method*, Artech House, 1998.
3. Kishk, A. A., *Electromagnetic Waves Propagation in Complex Matter*, InTech, 2011.
4. Atteia, G. E. and K. F. A. Hussein, "Realistic model of dispersive soils using PLRC-FDTD with applications to GPR systems," *Progress In Electromagnetics Research B*, Vol. 26, 335–359, 2010.
5. Prokopidis, K. P. and T. D. Tsiboukis, "Modeling of ground-penetrating radar for detecting buried objects in dispersive soils," *ACES Journal*, Vol. 22, No. 2, 289–292, Jul. 2007.
6. Liu, S.-X. and Z.-F. Zeng, "FDTD simulation for ground penetrating radar wave in dispersive medium," *Chinese Journal of Geophysics*, Vol. 50, No. 1, 299–306, 2007.
7. Uduwawala, D., M. Norgren, P. Fuks, and A. Gunawardena, "A complete FDTD simulation of a real GPR antenna system operating above lossy and dispersive grounds," *Progress In Electromagnetics Research*, Vol. 50, 209–229, 2005.
8. Ibrahim, K. M., K. F. A. Hussein, and A. A. Ammar, "Two-dimensional imaging and shape recognition of land buried objects through polarimetric ground penetrating radar," *The 2nd Middle East Conference on Antennas and Propagation "MECAP"*, 1–5, Cairo, Egypt, Dec. 2012.
9. Ibrahim, K. M., K. F. A. Hussein, and A. A. Ammar, "Reduction of noise effect in land-buried target shape recognition through polarimetric GPR images," *International Journal of Modern Engineering Research "IJMER"*, Vol. 3, No. 2, 1041–1055, Mar.–Apr. 2013.
10. Rothwell, E. J. and M. J. Cloud, *Electromagnetics*, Chapter 4, 189–348, CRC Press LLC, 2001.
11. Matin, M. A., *Ultra Wideband Communications: Novel Trends — Antennas and Propagation*, Chapter 6, 119–140, InTech, 2011.
12. Cossmann, S., E. Rothwell, and L. Kempel, "Transient reflection of TE-polarized plane waves from a lorentz-medium half-space," *Journal of the Optical Society of America, Series A*, Vol. 23, No. 9, 2320–2323, Sep. 2006.
13. Cossmann, S., E. Rothwell, and L. Kempel, "Transient reflection of TM-polarized plane waves from a lorentz-medium half-space," *Journal of the Optical Society of America, Series A*, Vol. 24, No. 3, 882–887, Mar. 2007.
14. Daniels, D. J., *Surface-penetrating Radar*, IEE, London, UK, 1996.
15. Matzler, C., "Microwave permittivity of dry sand," *IEEE Trans. on Geosci. Remote Sensing*, Vol. 36, 317–319, Jan. 1998.
16. Hipp, J. E., "Soil electromagnetic parameters as functions of frequency, density, and soil moisture," *Proc. IEEE*, Vol. 62, 98–103, Jan. 1974.